1-D Modelling of Pressure Fluctuations due to Confined Bubble Growth During Flow Boiling in a Microchannel

Sateesh GEDUPUDI, David B. R. KENNING, Tassos G. KARAYIANNIS *

* Corresponding author: Tel.: ++44 (0)1895 267132; Fax: ++44 (0)1895 256392
Email: tassos.karayiannis@brunel.ac.uk
School of Engineering and Design, Brunel University, UK

Abstract A simple 1-D model is presented to study the effects of the wall heat flux, location of the nucleation site, channel dimensions and fluid properties on the pressure fluctuations caused by confined bubble growth in rectangular microchannels, for zero upstream compressibility. A simple isothermal compressibility model is then used to study the effects of the initial volume of non-condensable gas trapped in the upstream plenum, initial inlet velocity and nucleation site location on local pressure fluctuations and transient flow reversal. Both acceleration pressure drop and viscous pressure drop are considered.

Keywords: Microchannel, Flow boiling, Confined bubble, Pressure fluctuation

1. Introduction

Better design of miniature two-phase microchannel heat sinks, intended for removal of heat fluxes exceeding l MW/m^2, demands a good understanding of pressure fluctuations and transient flow reversal caused by confined bubble growth during flow boiling in a microchannel.

A simple 1-D model for pressure fluctuation was developed by Kew and Cornwell (1996), considering the acceleration of the liquid slugs, and measurements by Kenning and Yan (2001) were of the same order as those estimated by Kew and Cornwell. Pressure fluctuations, dependent on the upstream compressibility arising from different sources, were measured by Zhang et al. (2004 and 2005) and Brutin and Tadrist (2004). Zhang et al. (2004) reported pressure fluctuations of up to 1.7 bar during boiling in a microchannel. Kenning et al. (2006) made measurements for the special case of bubble growth in an initially superheated channel with one sealed end. It was suggested by Kandlikar (2006) that a pressure spike associated with nucleation could cause flow reversal. A simplified model based on mass balance over the vapour bubble and over the liquid film, without taking into account the surface tension, friction and acceleration, was proposed by Rops et al. (2008) for explosive bubble growth during flow boiling in microchannels. A 1-D mechanistic model for a time-averaged pressure drop in the confined bubble regime was formulated by Shiferaw et al. (2009). A 1-D model for the pressure fluctuation during the bubble growth in two stages – partially confined and fully confined – was presented by Gedupudi et al. (2009a and 2009b) for zero and finite upstream compressibilities respectively. The present paper improves these models by including the viscous forces, bubble passage through the outlet and a non-linear model for upstream compressibility due to trapped gas. The transient fluctuations due to growth of a single bubble are modelled and are not time-averaged as in Shiferaw et al. (2009). The examples are mainly for water, with saturation properties at 1 bar. Other fluids are of interest to achieve lower temperatures.

2. 1-D Model for Confined Growth, No Upstream Compressibility

Bubble growth is assumed to occur in two stages – partially confined and fully confined, as shown in Fig. 1. The channel is of rectangular section, width w, depth h << w and heated length L_H. Heat input, q, is on one of the sides w, with an adiabatic window on the

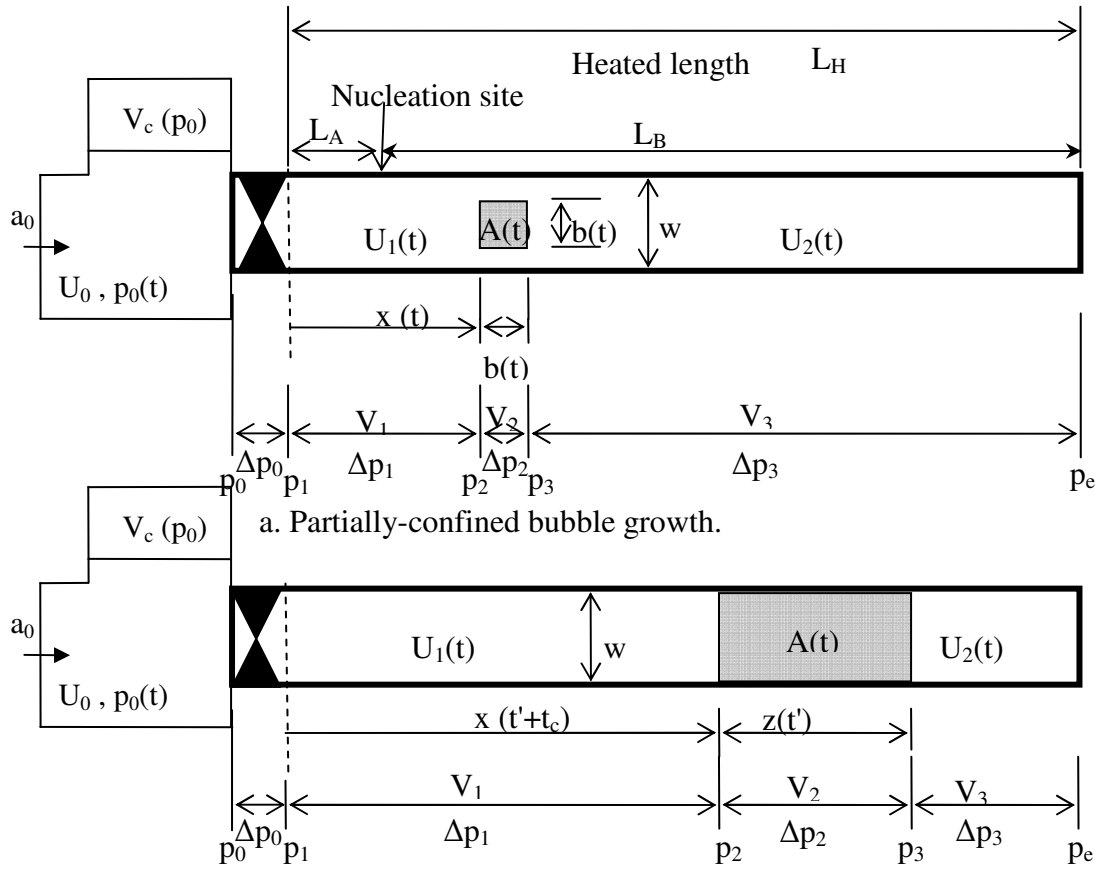

Fig. 1. Bubble growth models.

opposite side (as in visualization experiments) and negligible heat input on sides h. A single nucleation site is located at L_A from the inlet. A constant volumetric flow rate U_0a_0 is delivered by the pump to the upstream plenum of cross-sectional area $a_0 >> wh$ so that $p_0(t)$ is the stagnation pressure. When upstream compressibility is absent, $U_1 = U_0a_0/(wh)$.
All fluid properties, including ρ_v and h_{lv}, are assumed to be constant, evaluated at the constant channel outlet pressure p_e .

2.1 Partially-confined growth (PC)

Assuming constant heat flux q through the single contact area b^2,

$$b = he^{t/(2\tau)}, \qquad \tau = \rho_v h_{lv} h/q \tag{1}$$

From continuity,

$$U_2 = U_1 + \left(h^2/w\tau\right)e^{t/\tau} \tag{2}$$

The average velocities of the bubble and the liquid alongside are assumed to be equal to $(U_1+U_2)/2$. The following expression is obtained for the pressure drop from the law of conservation of momentum.

$$\frac{p_1(t) - p_e}{\rho_l} = \left(\frac{h^2}{w\tau^2}e^{t/\tau}\right)\left[\begin{array}{l} L_B - U_1\left(t - \dfrac{\rho_v\tau}{\rho_l}\right) \\ -\dfrac{3}{4}he^{t/(2\tau)} + \dfrac{\rho_v}{\rho_l}\dfrac{h^2}{w}e^{t/\tau}\end{array}\right] + \frac{\Delta p_f}{\rho_l} \tag{3}$$

The time required for confinement, t_c, from b = h (at time t = 0) to b = w (at time $t = t_c$) is

$$t_c = 2\,\tau \ln (w/h) \tag{4}$$

2.2 Fully-confined growth (FC)

Fully-confined bubble growth starts from the time t_c at which b = w. Let $t' = t - t_c$. The contact area A = w z (t'), where z is the length of the bubble. The expression for z can be obtained as

$$z = we^{t'/\tau} \tag{5}$$

From continuity,

$$U_2 = U_1 + \frac{dz}{dt'} = U_1 + \left(\frac{w}{\tau}\right)e^{t'/\tau} \tag{6}$$

The expression for pressure drop is

$$\frac{p_l(t)-p_e}{\rho_l}=\left(\frac{w}{\tau^2}e^{t'/\tau}\right)\left[L_B-U_l(t'+t_c)-we^{t'/\tau}\right]+\left(\frac{\rho_v}{\rho_l}\right)\left[U_l\left(\frac{w}{\tau}e^{t'/\tau}\right)+\left(\frac{w}{\tau}\right)^2e^{2t'/\tau}\right]+\frac{\Delta p_f}{\rho_l} \quad (7)$$

More detailed derivation (without frictional pressure drop, Δp_f) for PC and FC is given by Gedupudi et al. (2009a).

2.3 Bubble passage through the outlet (OL)

From the moment the downstream end of the fully confined bubble reaches the channel outlet, the length over which evaporation occurs is limited by the upstream liquid velocity. That is,

$$\frac{dz}{dt}=-U_l \quad (8)$$

The heat balance gives

$$U_2=U_l+\frac{z}{\tau} \quad (9)$$

where U_2 is now the vapour exit velocity.
The pressure drop across the channel is

$$\frac{p_l(t)-p_e}{\rho_l}=\frac{\rho_v}{\rho_l}\left(\frac{z^2}{\tau^2}+U_l\frac{z}{\tau}\right)+\frac{\Delta p_f}{\rho_l} \quad (10)$$

2.4 Viscous pressure drop (Δp_f)

The friction factor correlations available in literature are mainly for steady flow, but flows in boiling involve large accelerations and reversals. There is also some doubt about the laminar-turbulent transition in micro-channels. As a simple first estimate, an expression for the Fanning friction factor f_F as a function of Reynolds number Re and the channel aspect ratio α in steady laminar flow from Paputsky et al. (1999), White (1994) and Hartnett and Kostic (1989), (after conversion from Darcy friction factor $f_D = 4f_F$), is combined with a minimum Fanning friction factor $f_F = 0.01$ for turbulent flow. On a Moody chart, this corresponds to transition at about Re = 1500 and a relative roughness of ~ 10^{-2}. This is very approximate.

$$f_F Re = 24(1-1.3553\alpha+1.9467\alpha^2-1.7012\alpha^3+0.9564\alpha^4-0.2537\alpha^5)$$

where $0<\alpha<1$. (11)

The viscous pressure drop considered here occurs only in the liquid slugs upstream and downstream of the bubble, of lengths L_u and L_d. The total viscous pressure drop is given by

$$\Delta p_f=\Delta p_{f,u}+\Delta p_{f,d} \quad (12)$$

where

$$\Delta p_{f,u}=S_1\frac{2\rho_l f_{F,u}L_u U_l^2}{D_h} \quad (13)$$

$$\Delta p_{f,d}=S_2\frac{2\rho_l f_{F,d}L_d U_2^2}{D_h} \quad (14)$$

where $S_1 = |U_1| / U_1$, $S_2 = |U_2| / U_2$
Stagnation pressure p_0 is given by

$$p_0=p_l+(1.5K)\frac{\rho_l U_l^2}{2} \quad (15)$$

with minor loss at the channel entry, equal to $\frac{1}{2}\left(\frac{\rho_l U_l^2}{2}\right)$, included in the above expression.

K=1 for positive U_1 and equal to 0 for negative U_1(possible with upstream compressibility).

2.5 Simulations with constant properties

Zhang et al. (2004) observed pressure fluctuations with amplitudes ranging from 0.86 bar to 1.72 bar, during flow boiling of water in a 0.113 mm D_h (0.1mm wide and 0.13 mm deep) and 20mm long channel, with volume flow rate 0.1 ml/min (0.13 m/s) and heat flux about 110kW/m^2. Modelling results for similar conditions are shown in Fig. 2. Peak transient pressure drops are 3.59, 0.57 and 0.18 bar for nucleation at the inlet, 10mm away and 14mm away respectively. In recent calculations using pressure-dependent properties in the model, as

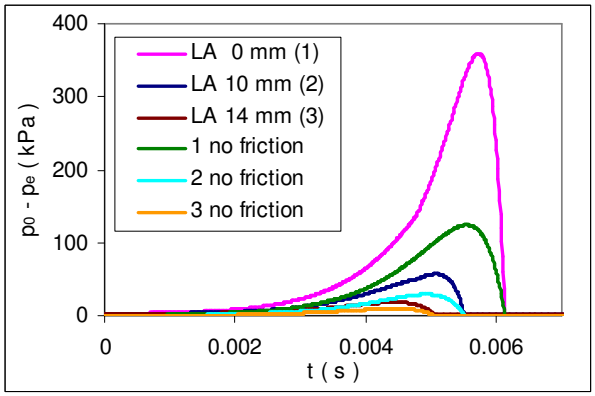

Fig. 2. p_0 - p_e drop for different locations of nucleation site (L_A). Channel 0.07 x 0.35 x 20 mm, q = 110 kW/m^2, U_1 = 0.13m/s, p_e = 1 bar.

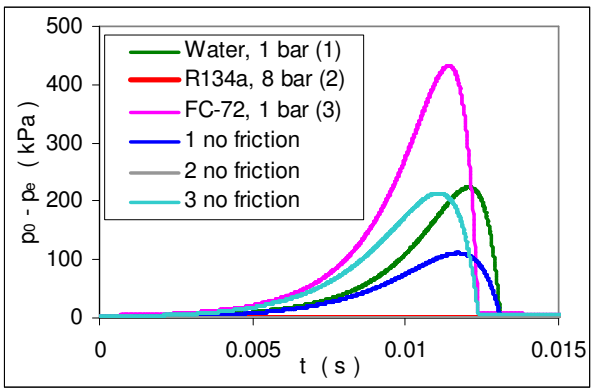

Fig. 3. Transient pressure drop for different fluids in a channel 0.3 x 1.5 x 50 mm, q = 200 kW/m^2, U_1 = 0.6m/s. L_A = 0mm.

in Gedupudi et al. (2009a) but with friction now included, the peak values become 0.93 bar for L_A = 0 and 0.34 bar for L_A = 10 mm, in reasonable agreement with those observed by Zhang et al. For a much higher heat flux of 2MW/m^2 to water in a shorter channel 0.15 x 0.75 x 10 mm (L/D_h = 40), the values of the peak transient pressure drop with constant and variable properties (for L_A = 0 mm) are 32 bar and 2.6 bar respectively; they are the same for a 0.3 x 1.5 x 20 mm channel (L/D_h = 40). Velocities and accelerations depend inversely on the product ($\rho_v h_{lv}$) in Eqn. (1). The ratios of the peak absolute pressures are roughly proportional to the ratios by which the constant property model underestimates this product. The constant property model is quicker to run and can be expected to conservatively identify the conditions leading to large pressure fluctuations.

The influence of fluid properties, particularly ($\rho_v h_{lv}$), is also seen in Fig. 3, with large peak pressures for water and FC-72 at 1 bar and negligible change in pressure for R134a at 8 bar with a much larger value of ($\rho_v h_{lv}$).

Figs. 2, 3, and Fig. 9c later, show that frictional and acceleration pressure drops make similar contributions to the peak transient pressure. Property variation must be included for more accurate assessment.

3. Upstream Compressibility

A common phenomenon observed during flow boiling in micro-channels is transient flow reversal, caused by the transient pressure fluctuations due to confined bubble growth. This flow reversal can only occur if there is upstream compressibility, sources of which include pump characteristics, non-condensable gas trapped in the upstream plenum, subcooled boiling creating a condensable void upstream of the channel, in-channel compressibility (due to multiple bubbles in the channel) or connections through inlet and outlet headers to parallel channels (as required in most microchannel heat sinks).

Flow reversal can result in lower critical heat flux (CHF) and push vapour into other channels through the inlet header, causing transient dry-out. Modelling this flow reversal can assist in a better design of two-phase microchannel heat sinks.

In this paper, non-condensable gas of initial volume V_c is assumed to be trapped in the inlet plenum, as shown in Fig. 1. At present, the model stops if the gas expands sufficiently to enter the channel, or if the upstream end of the vapour bubble in the channel reaches the channel inlet during reverse flow.

From the continuity equation,

$$(U_0 a_0) + (dV_c/dt) = whU_1 \qquad (16)$$

Assuming the trapped gas is compressed isothermally,

$$p_0 V_c = p_{0i} V_{ci} = C \qquad (17)$$

From (15), (16) and (17),

$$\frac{dp_1}{dt} = \frac{p_0^2}{C}\left(a_0 U_0 - whU_1\right) - \left(1.5K\right)\rho_1 U_1 \frac{dU_1}{dt} \qquad (18)$$

$$U_1 = dx/dt \qquad (19)$$

For PC growth, pressure differences, as shown in Fig. 1, are given by

$$\Delta p_1 = \rho_1\left(x\frac{dU_1}{dt}\right) + \Delta p_{f,u} \qquad (20)$$

$$\Delta p_2 = \left\{\begin{array}{l}\left[\left(\rho_1\frac{db}{dt}\right) - \left(\rho_1 - \rho_v\right)\frac{2b}{w}\frac{db}{dt}\right]\frac{\left(U_1 + U_2\right)}{2} \\ + \left[\left(\rho_1 b\right) - \left(\rho_1 - \rho_v\right)\frac{b^2}{w}\right]\frac{1}{2}\left(\frac{dU_1}{dt} + \frac{dU_2}{dt}\right)\end{array}\right\} \qquad (21)$$

$$\Delta p_3 = \rho_l\left[U_2\left(- U_1 - \frac{db}{dt}\right) + \left(L_H - x - b\right)\frac{dU_2}{dt}\right] + \left[\rho_l U_2^2 - 0\right] + \Delta p_{f,d} \qquad (22)$$

From the above equations, with r as the ratio of vapour density to liquid density, ρ_v / ρ_l ,

$$\frac{dU_1}{dt} = \frac{\left(\begin{array}{l} \frac{p_1 - p_e}{\rho_l} - \frac{\Delta p_f}{\rho_l} - U_1\left[r\frac{h^2}{w\tau} e^{t/\tau}\right] \\ - e^{t/\tau}\frac{h^2}{w\tau^2}(L_H - x) + e^{3t/2\tau}\frac{3h^3}{4w\tau^2} \\ - e^{2t/\tau}\frac{h^4}{w^2\tau^2} r \end{array}\right)}{\left[L_H - (1-r)\frac{h^2}{w} e^{t/\tau}\right]} \qquad (23)$$

For FC growth, pressure differences, as shown in Fig. 1, are given by

$$\Delta p_1 = \rho_l\left(x\frac{dU_1}{dt}\right) + \Delta p_{f,u} \qquad (24)$$

$$\Delta p_2 = \left\{\begin{array}{l}\left[\left(\rho_v \frac{dz}{dt}\right)\frac{(U_1 + U_2)}{2}\right] \\ + \left[(\rho_v z)\frac{1}{2}\left(\frac{dU_1}{dt} + \frac{dU_2}{dt}\right)\right]\end{array}\right\} \qquad (25)$$

$$\Delta p_3 = \rho_l\left[(L_H - x - z)\frac{dU_2}{dt}\right] + \Delta p_{f,d} \qquad (26)$$

$$\frac{dU_1}{dt'} = \frac{\left(\begin{array}{l} \frac{p_1 - p_e}{\rho_l} - \frac{\Delta p_f}{\rho_l} - U_1\frac{rw}{\tau} e^{t'/\tau} \\ - (L_H - x)\frac{w}{\tau^2} e^{t'/\tau} + (1-r)\frac{w^2}{\tau^2} e^{2t'/\tau} \end{array}\right)}{\left[L_H - (1-r) w e^{t'/\tau}\right]} \qquad (27)$$

For bubble passage through the channel outlet,

$$\frac{dU_1}{dt} = \frac{(p_1 - p_e) - (\Delta p_f) - \rho_v\left(\frac{z^2}{\tau^2} + U_1\frac{z}{\tau}\right)}{\rho_l x + \rho_v z} \qquad (28)$$

The equations are solved by a finite difference method. The incoming flow a_0U_0 and the exit pressure p_e are assumed to be constant. The initial conditions are assumed to be $p_1 = p_e$, $U_1 = a_0U_0 / wh$, neglecting any impulsive changes associated with the initial unconfined growth of the bubble. Bubble growth rate equations and expressions for U_2 are the same as in section 2 for constant vapour properties.

The following examples are for water, with properties corresponding to constant outlet pressure of 1 bar in a channel 0.3x1.5x50 mm, volume 22.5 mm^3. The initial volumes of compressible gas, V_{ci}, are chosen to be equal to the channel volume times factors 0.1, 2, 40. From eqn. (17), the values of $C = p_{0i}V_{ci}$ are

$C_1 = 0$ (incompressible)

$C_2 = 1x10^5$ x 22.5 x 10^{-9} x (0.1)
$= 2.25$ x 10^{-4} Nm

$C_3 = 10^5$ x 22.5 x 10^{-9} x (2) $= 4.50$ x 10^{-3} Nm

$C_4 = 10^5$ x 22.5 x 10^{-9} x (40) = 0.09 Nm

Fig. 4 shows the upstream and downstream locations of a bubble initiated at the channel mid-point L_A = 25 mm for initial U_1 = 0.2m/s, q = 200kW/m^2 for different values of C. With C equal to 2.25 x 10^{-4} and 4.5 x 10^{-3} Nm, the upstream end of the bubble fluctuates; with C = 0.09Nm, it reverses completely and reaches the channel inlet and the model stops at 0.015s. The frequencies of fluctuations shown in Fig. 5 as the liquid column progresses towards the downstream end of the channel are in good agreement with the natural frequency n of a spring-mass system using the upstream mass of the liquid column in the channel, given by

$n = (wh/\rho L\alpha)^{1/2} /2\pi$, where $\alpha = -dV_c / dp_0$ (29)

e.g.

$p_0V_c = C$, $\alpha = C / (p_o)^2$

average p_o ~ 100 kPa

average liquid column length L= (25+50)/2 = 37.5mm, w=1.5mm, h=0.3mm.

C_2 : n = 116/s, period 8.6 ms

C_3 : n = 26/s, period 38 ms

These values match well with those in Fig. 5.

Increasing the compressibility C causes considerable reduction in the peak pressure difference across the channel, Fig. 5, but there are only small changes in the peak pressure $p_3 - p_e$, Fig. 6.

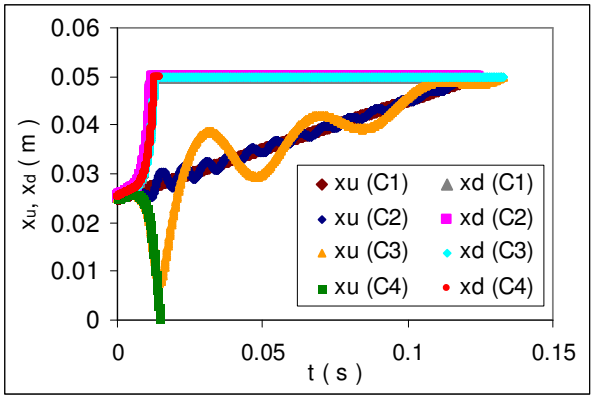

Fig. 4. Bubble upstream and downstream locations (x_u and x_d) for different C values. q = 200 kW/m^2, $U_1(0)$ = 0.2m/s. L_A = 25mm. Water at 1 bar in channel 0.3x1.5x50 mm.

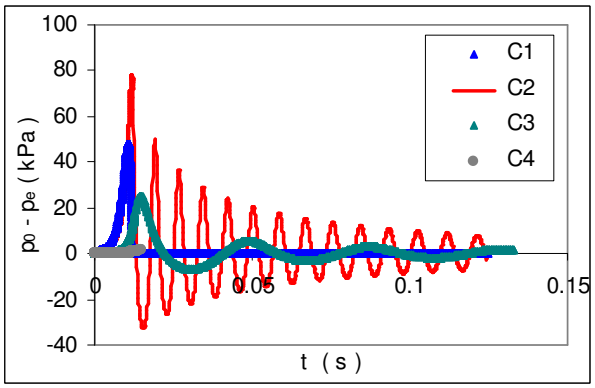

Fig. 5. p_0 - p_e for different C values. q = 200 kW/m^2, $U_1(0)$ = 0.2m/s. L_A = 25mm.

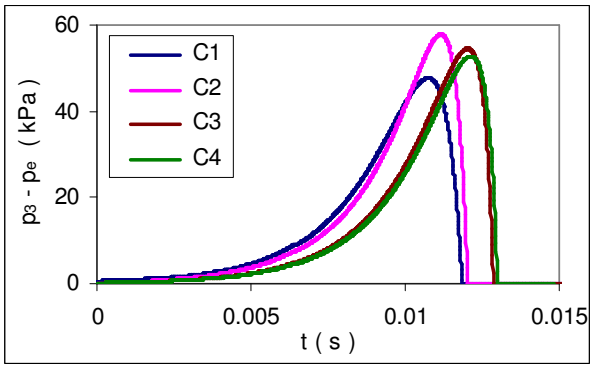

Fig. 6. p_3 - p_e for different C values. q = 200 kW/m^2, $U_1(0)$ = 0.2m/s. L_A = 25mm.

Nucleation sites closer to the inlet show more tendency for reverse flow, Fig. 7, as the liquid inertial and frictional resistances downstream of the bubble will be higher. Fig. 8 shows that the peak pressure p_3-p_e is higher for the nucleation site at the channel middle (25mm) than for sites near the inlet and outlet. Sites

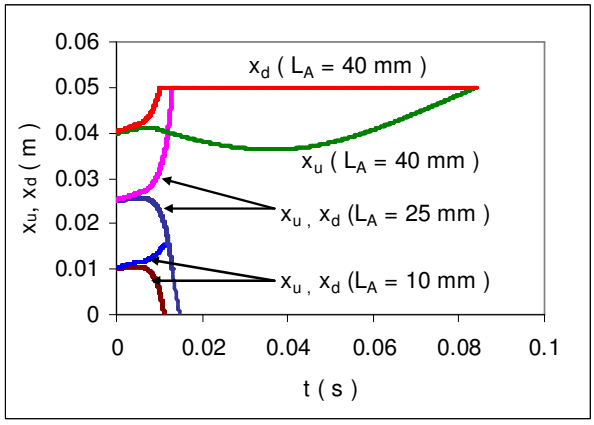

Fig. 7. x_u and x_d for different L_A values. q = 200 kW/m^2, $U_1(0)$ = 0.2m/s. C = C_4.

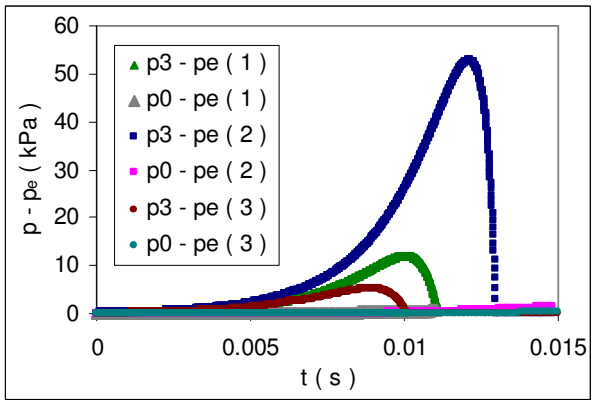

Fig. 8. p_3 - p_e and p_0 - p_e for L_A = 10 (1), 25 (2) and 40 mm (3). q = 200 kW/m^2, $U_1(0)$ = 0.2m/s. C = C_4.

near the inlet promote flow reversal, reducing the acceleration dU_2/dt of the downstream slug. Bubbles from sites near the outlet have less mass of liquid in the downstream slug and reach the exit quickly. In all the examples with compressibility and flow reversal, for V_{ci} > channel volume (C_3 and C_4), the pressure drop across the channel, p_0-p_e, is very low compared to the local pressure fluctuation p_3-p_e, because reversal causes a negative pressure drop at the upstream side that partially balances the positive pressure drop at the downstream side, as can also be seen in Fig. 9c, near the peak in p_3-p_e .

Fig. 9 shows the bubble location, liquid velocities (U_1 and U_2) and the pressure drop, all with and without friction. The second flow reversal (bubble forward motion after backward motion) commences during the passage of the downstream end of the bubble

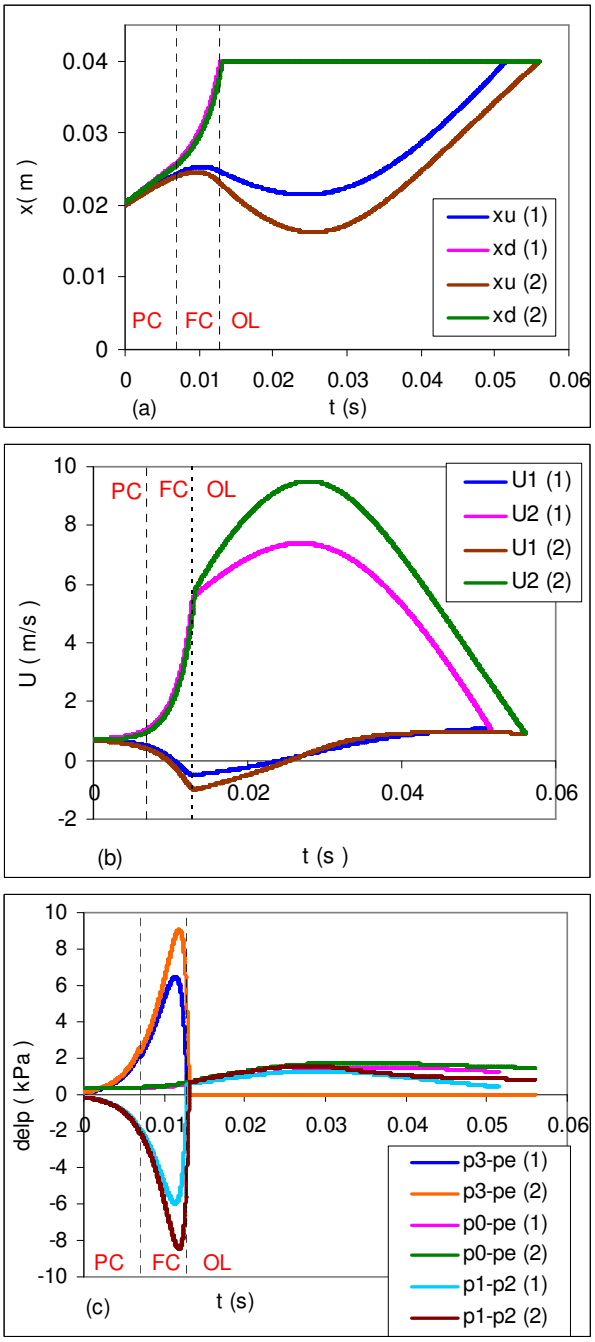

Fig. 9. (a) x_u and x_d (b) U_1 and U_2 (c) pressure drop, without (1) and with (2) friction. Channel 0.38 x 1.5 x 40 mm, L_A = 20 mm, q = 200 kW/m^2, $U_1(0)$ = 0.7m/s. C = 0.1Nm.

through the outlet, Figs. 9 and 10. Lower initial upstream liquid velocity means lower inertia of the upstream liquid slug, which promotes flow reversal, Fig. 10.

Conclusions

A simple 1-D model, considering both acceleration pressure drop and viscous

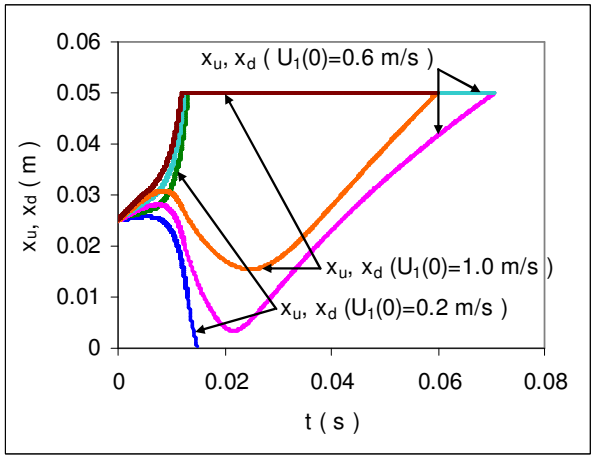

Fig. 10. x_u and x_d for different $U_1(0)$ values. q = 200 kW/m^2, L_A = 25mm. C = C_4.

pressure drop is presented. Using this model, the effect of upstream compressibility, caused by non-condensable gas, on the transient flow reversal and pressure fluctuation has been studied. The simulations show that, with upstream compressibility, the local transient pressure fluctuation can be much higher than that measured across the channel. The volume of the non-condensable gas, the initial upstream velocity and location of the nucleation site all have major influences on the transient flow reversal. Results also demonstrate the need to ensure that the pressure tappings, tubing and connections used for transient pressure measurements with the pressure transducers are free of trapped vapour or non-condensable gas, to eliminate the compressibility and viscous damping, which otherwise result in erroneous measurement of the fluctuation amplitudes. Structurally integrated strain gauges may be the better choice for transient pressure measurements, provided the pressure and temperature sensitivities of the gauges can be decoupled.

The effect of upstream compressibility caused by other sources such as sub-cooled void will be studied later. Further development of the model is required to include pressure-dependent vapour properties to study the effect of heat flux over a wide range, and to include the dimensions of the inlet restriction (which can reduce flow reversal) and to include multiple bubbles (which also cause in-channel compressibility) and variable nucleation

frequencies along the channel. The model must be extended to cover repeated bubble cycles.

The examples presented here also show that for an accurate experimental validation of the model developed for single bubble, it is essential to have only a single nucleation site (or bubble) in the channel. The presence of multiple bubbles (possibly with different nucleation frequencies) in the channel causes in-channel compressibility and affects the acceleration and length of the liquid slug(s), all of which influence the transient pressure.

Acknowledgement

This work was supported by the Engineering and Physical Sciences Research Council, Grant EP/D500095/1.

References

Kew, P.A., Cornwell, K., 1996. On pressure fluctuations during boiling in narrow channels, Proc. 2nd European Thermal Sciences and 14th UIT National Heat Transfer Conf., Rome, vol. 3, 1323-1327.

Kenning, D.B.R., Yan, Y., 2001. Saturated flow boiling of water in a narrow channel: experimental investigation of local phenomena, IChemE Trans. A, Chem. Eng. Res. And Design, 79, 425-436.

Zhang, L., Goodson, K.E., Kenny, T.W., 2004. Silicon Microchannel Heat Sinks, Theories and Phenomena, Springer Verlag, Berlin, Heidelberg, New York.

Zhang, L., Wang, E.N., Goodson, K.E., Kenny, T.W., 2005. Phase change phenomena in silicon microchannels, Int. J. Heat Mass Transfer 48, 1572–1582.

Brutin, D., Tadrist, L., 2004. Pressure drop and heat transfer analysis of flow boiling in a minichannel; influence of the inlet condition on two-phase flow stability, Int. J. Heat Mass Transfer 47, 2365-2377.

Kenning, D.B.R., Wen, D.S., Das, K.S., Wilson, S.K., 2006. Confined growth of a vapour bubble in a capillary tube at initially uniform superheat: experiments and modelling, Int. J. Heat Mass Transfer 49, 4653-4671.

Kandlikar, S.G., 2006. Nucleation characteristics and stability considerations during flow boiling in microchannels, Experimental Thermal and Fluid Science, 30, 441-447.

Rops, C.M., Geers, L.F.G., Lindken, R., Westerweel, J., 2008. Explosive bubble growth during flow boiling in micro-channels, 5th European Thermal-Sciences Conference, The Netherlands, 2008.

Shiferaw, D., Mahmoud, M., Karayiannis, T.G., Kenning, D.B.R., 2009. One-dimensional mechanistic model for flow boiling pressure drop in small-to micro-passages, 2nd Micro and Nano Flows Conference, West London, U.K., 1-2 September 2009.

Gedupudi, S., Zu, Y.Q., Karayiannis, T.G., Kenning, D.B.R., Yan, Y.Y., 2009a. 1-D modelling and 3-D simulation of confined bubble formation and pressure fluctuations during flow boiling in a mini-micro channel with a rectangular cross-section of high aspect ratio, Proc. 7th Int. ASME Conf. on Nanochannels, Microchannels and Minichannels, paper no. ICNMM2009-82119, Pohang, June 22-24, 2009.

Gedupudi, S., Karayiannis, T.G., Kenning, D.B.R., 2009b. Modelling pressure fluctuations during flow boiling in microchannels with inlet compressibility and resistance, Proc. 7th World Conference on Experimental Heat Transfer, Fluid Mechanics and Thermodynamics, Krakow, Poland, 28 June – 03 July 2009.

Hartnett, J. P., Kostic, M., 1989. Heat transfer to Newtonian and non-Newtonian fluids in rectangular ducts, Advances in Heat Transfer 19, 247-356.

Papautsky, I., Gale, B. K., Mohanty, S., Ameel, T. A., Frazier, A.B., 1999. Effects of rectangular microchannel aspect ratio on laminar friction constant, Proc. SPIE Symposium on Micromachining and Microfabrication: MicroFluidic Devices and Systems, Santa Clara, CA, Sep. 20-21, 1999, pp. 147-158.

White, F. M., 1994. Fluid Mechanics, 3rd ed., New York, NY: McGraw Hill.